BMC Urology

RESEARCH Open Access

KIF14 plays a role in the regulation of the cell cycle and has implications for prognosis in clear cell renal cell carcinoma

Jie Wang[1*†], Xuejia Lai[1†], Zhijun Sun[1], Sike Feng[1], Bi Li[1] and Hu Zhao[2*]

Abstract

Background Kinesin family member 14 (KIF14) is a significant multifunctional protein that has been linked to several malignancies. However, the varied expression profiles of KIF14 and its prognostic relevance in Clear cell renal cell carcinoma (ccRCC) have yet to be elucidated.

Methods Patients with ccRCC were obtained from The Cancer Genome Atlas (TCGA), Gene Expression Omnibus (GEO) and ArrayExpress databases. A comparison of KIF14 expression levels between ccRCC and normal tissues was conducted using the Wilcoxon rank sum test. Logistic regression analysis was subsequently employed to evaluate the relationship between KIF14 expression and clinicopathological features. Furthermore, Gene Ontology (GO) and Kyoto Encyclopedia of Genes and Genomes (KEGG) term analysis, gene set enrichment analysis (GSEA) and single sample gene set enrichment analysis (ssGSEA), as well as CIBERSORT, were utilized to elucidate the enriched pathways and functions linked to KIF14 and to quantify the level of immune cell infiltration. Kaplan-Meier analysis was conducted to assess the correlation between KIF14 expression and survival. Additionally, KIF14 expression was downregulated in A498 ccRCC cells, and their proliferation, expansion capacity, cell cycle, and apoptosis were assessed through CCK-8 assays, colony formation assays, 7-AAD staining, and Annexin V/PI staining, respectively.

Results The findings of this study demonstrate that KIF14 mRNA levels are notably increased in ccRCC. Furthermore, a positive association was observed between KIF14 expression and cancer stage, nodal metastasis, and the infiltration of various immune cells in ccRCC. High levels of KIF14 were also found to be indicative of poor survival outcomes among ccRCC patients. Knockdown of KIF14 in A498 cells resulted in reduced proliferation, diminished colony formation capacity, cell cycle arrest, increased apoptosis, and downregulation of CyclinD1 and CDK4.

Conclusions KIF14 down-regulates cell cycle proteins CyclinD1 and CDK4 to facilitate the proliferation of ccRCC cells, suggesting its potential as a therapeutic target and prognostic biomarker in ccRCC.

Keywords KIF14, Clear cell renal cell carcinoma, Immune infiltration, Proliferation, Cell cycle

[†]Jie Wang and Xuejia Lai contributed as the first co-authors.

*Correspondence:
Jie Wang
ddcsw000@stu.xmu.edu.cn; ddcsw000@gmail.com

Hu Zhao
zhaohubear@163.com
[1]Department of Urology, Ningbo Ninth Hospital, No.68, Xiangbei Road, Ningbo, Zhejiang 315000, PR China
[2]Department of General Surgery, 900 Hospital of the Joint Logistics Support Force, 156 Xierhuan Road, Fuzhou, Fujian 350025, PR China

Introduction

Renal cell carcinoma (RCC), representing 85% of renal cancers and 2–3% of adult malignancies [1], saw 431,288 new cases and 179,368 deaths globally in 2020 (GLOBOCAN data) [2, 3]. Clear cell RCC (ccRCC), the predominant (70%) and most aggressive subtype [4], often remains asymptomatic until advanced stages. While surgical resection remains primary treatment for localized cases, ~30% experience recurrence and high mortality upon metastasis [5, 6]. Despite recent survival improvements through targeted therapies and immunotherapy, challenges persist in understanding tumor heterogeneity, immune evasion mechanisms, and personalizing treatment strategies [7, 8]. This underscores the critical need to identify novel biomarkers and therapeutic targets for ccRCC.

Kinesin superfamily proteins (KIFs) are ATP-dependent molecular motors that transport a variety of cargoes along microtubules in cells and are fundamental to cellular function and morphogenesis. They are divided into 14 different families, each with distinct structural and functional properties [9]. These molecular motors are ubiquitously expressed and play key roles in organelle and vesicle trafficking, mitosis, spindle assembly and chromosome aggregation [10]. However, there is increasing evidence that KIFs are involved in cancer development as potential biomarkers. Kinesin family member 14 (KIF14), a member of the KIFs family, is a protein-coding gene. This gene encodes a member of the kinesin-3 superfamily of microtubule-moving proteins, which are involved in many processes including vesicle transport, chromosome segregation, mitotic spindle formation and cytokinesis [11]. Overexpression of KIF14 can lead to rapid and error-prone mitosis, thereby inducing DNA aneuploidy during tumorigenesis [12]. In recent years, a growing body of evidence has shown that KIF14 is closely associated with the pathogenesis of many malignancies, including clear cell renal cell carcinoma [13], thyroid carcinoma [14], and colorectal cancer [15]. Fang's research revealed that the deletion of KIF14 induces apoptosis, inhibits cell growth, migration, and invasion via the PI3K/AKT pathway in bladder cancer [16]. By suppressing KIF14 expression, resistant prostate cancer cells can regain sensitivity to both docetaxel and cabazitaxel, while also exhibiting reduced proliferation and increased apoptosis [17]. In cervical cancer, KIF14 overexpression activates the cell cycle and cell viability by blocking p27 degradation [18]. Similarly, in hepatocellular carcinoma, KIF14 knockdown disrupts cytokinesis by impairing the ubiquitination-dependent degradation of Kip1 [19]. Despite these advances, the role of KIF14 in ccRCC remains poorly defined. Current studies predominantly focus on KIF14's mitotic functions, yet its prognostic significance, immune-modulatory roles, and interaction with key cell cycle regulators (e.g., CyclinD1/CDK4) in ccRCC are unexplored. Notably, while KIF14 overexpression correlates with poor survival in cancer patients [20], no study has systematically linked its expression to advanced clinicopathological features (e.g., metastasis, immune evasion) in ccRCC. This gap is critical because ccRCC exhibits immune microenvironment characteristics [21], which may render KIF14 a context-dependent oncogene. Addressing these questions could uncover novel biomarkers to stratify high-risk patients or synergize with immunotherapy.

In this study, we investigated the expression of KIF14 in renal clear cell carcinoma using a bioinformatics approach by obtaining transcriptomic data from The Cancer Genome Atlas (TCGA), Gene Expression Omnibus (GEO) and ArrayExpress databases. Specifically, our analyses focused on KIF14 expression in ccRCC and its correlation with clinicopathological features, prognosis and immune infiltration status of ccRCC, as well as functional analyses. We also performed functional studies of KIF14 in A498 ccRCC cells. Our data showed that KIF14 was overexpressed in ccRCC and exhibited oncogenic function in A498 cells. These findings contribute to our understanding of the role of KIF14 in the development of ccRCC.

Materials and methods

TCGA data source and preprocessing

RNA-sequencing expression profiles (level 3 HTSeq-FPKM) profiles and miRNA data (level HTSeq-RPM) and corresponding clinical information [22] for KIRC were downloaded from the TCGA dataset (https://portal.gdc.com). Filtered clinical information: Normal KIRC cohort, duplicate samples and overall survival less than 30 days were removed. Next, RNAseq data in FPKM format were converted to TPM (transcripts per million reads) and then log2 transformed. Simultaneously, miRNAseq data in RPM format were log2 transformed. The final TCGA data, which included 72 normal tissues and 530 tumor tissues (TPM data) and 71 normal tissues and 516 tumor tissues (RPM data) were used for further analyses. The R software (version 4.1.0) was used to process the for TCGA data processing. The study followed the TCGA guidelines.

GEO database and the arrayexpress database validation

Three microarray expression datasets, GSE15641, GSE40435, GSE16441 were downloaded from the GEO database (http://www.ncbi.nih.gov/geo). All the raw data were downloaded as series matrix files. GSE15641 included 32 ccRCC patients and 23 normal patients; GSE40435 included 101 pairs of ccRCC tumours and adjacent non-tumour renal tissue; GSE16441 consisted of 17 ccRCC tumors and 17 corresponding non-tumor

samples. Filtered data: For genes with multiple probes, the probe with the highest expression value (on average) was retained. For small-sample datasets, non-parametric tests (Wilcoxon rank-sum for unpaired data; Wilcoxon signed-rank for paired data) were applied to mitigate normality assumptions. Statistical significance was defined as $p < 0.05$ after false discovery rate (FDR) correction. The microarray expression of E-MTAB-1805 was downloaded from the ArrayExpress database (https://www.ebi.ac.uk/arrayexpress/) and included 15 normal tissues and 105 ccRCC tissues.

KIF14 differential expression in ccRCC tissues

Boxplots and scatter plots, using the ggplot2 package for plotting, were used to represent the differential expression of KIF14 in ccRCC. For TCGA KIRC specimens, Wilcoxon rank sum test for unpaired samples and Wilcoxon signed rank test for paired samples were performed; Wilcoxon rank sum test was performed for GSE15641 dataset specimens; Wilcoxon signed rank test were used for GSE40435 dataset specimens; paired sample t-Test was performed for GSE16441 dataset specimens. Receiver Operating Characteristic (ROC) curves were plotted using the pROC and ggplot2 packages to investigate the diagnostic validity of KIF14.

Functional enrichment analysis

To clarify the potential biological functions of KIF14 in ccRCC, the guilt by association analysis was conducted. We performed a Spearman correlation analysis of KIF14 by gene in TCGA KIRC expression profiling. Results with absolute correlation coefficient (cor) > 0.5 & p-values < 0.001 were considered as statistically significant correlation. Next, we conducted the Gene Ontology (GO) and Kyoto Encyclopedia of Genes and Genomes (KEGG) pathway enrichment analyses were then performed for KIF14-related genes. The enrichment analysis was performed using the clusterProfiler (version4.4.4) R package [23] and Metascape [24]. The threshold conditions of enrichment results included: adjusted *P*-value (*p*.adjust) < 0.05 & false discovery rate (FDR) < 0.2 was considered statistically significant. Gene set enrichment analysis (GSEA) [25]was used to elucidate the significant functional and pathway differences between the high and low KIF14 expression groups. Hallmark gene sets was called and each analysis procedure was repeated 1000 times, with each gene set containing at least 10 genes. Finally, A function or pathway term with *p*.adjust < 0.05 & FDR < 0.25 was considered statistically significant.

Analysis of immune cell infiltration and tumor immune escape

We undertook immune infiltration analysis for TCGA KIRC sample genes using single-sample GSEA (ssGSEA) and CIBERSORT [26] methods to assess the relative levels tumor infiltration. ssGSEA analysis was performed using the GSVA R package [27] for 24 immunocytes types in published signature gene lists [28]; the proportions of the 22 infiltrating immune cells present in the LM22 datasets from each sample were calculated by using the CIBERSORT R package. To better assess the distribution of stromal and immune cells in the tumor microenvironment, the total StromalScore, ImmuneScore, and ESTIMATEScore were determined from each sample using the estimate R package [29]. To explore the relationship between KIF14 and the infiltration levels of each immune cell subset, Spearman correlations were applied. Moreover, the association of immunocytes infiltration with low and high KIF14 expression groups was investigated using the Wilcoxon rank sum test.

Understanding the mechanism of tumor immune has important implications for tumor treatment, especially implications for cancer immunotherapy. Based on the Tumor Immune Dysfunction and Exclusion (TIDE) algorithm, we estimate the immunotherapy response with low and high KIF14 expression groups in the TCGA-KIRC dataset. The TIDE score of patients with TCGA KIRC was obtained from the TIDE website (http://tide.dfci.harvard.edu) after uploading the RNA-sequencing expression profiles. Wilcoxon rank sum test was performed to investigate the association of TIDE score with low and high KIF14 expression groups. Furthermore, the relationship between the different expression groups of KIF14 and cancer associated fibroblast-TIDE was evaluated by utilizing TIMER2 (http://timer.cistrome.org) database.

Clinical statistical and survival analysis

The association of clinicalpathologic features with KIF14 was analyzed using Chi-squared test and logistic regression. Cox regression analysis was performed to explore the relevance between different KIF14 groups expression and overall survival (OS), progression-free interval (PFI), and disease-specific survival (DSS) in patient prognosis using the survival R package. A cut-off value of 50% was set as the KIF14 expression threshold to separating high and low expression cohorts. The Kaplan-Meier survival curve was plotted by using the survminer R package. *P*-value, hazard ratio (HR), and 95% confidence intervals were investigated.

Cell culture and SiRNA transfection

All cell lines (ACHN, A498 and 786-O) were sourced from IMMOCELL (Xiamen, Fujian, China). ACHN and A498 cells were cultured in DMEM with 10% fetal bovine serum (Gibco), while 786-O cell were cultured in RPMI 1640 medium with 10% fetal bovine serum. These cells were maintained in a humidified incubator at 37 °C with

Table 1 The SiRNA sequences of KIF14

Serial number	siRNA name	siRNA sequences
1	siKIF14-1-F	5′-GGAUGAGUUGAGACAAGAATT-3′
2	siKIF14-1-R	5′-UUCUUGUCUCAACUCAUCCTT-3′
3	siKIF14-2-F	5′-GACUGAAGUUGUUAGAUCATT-3′
4	siKIF14-2-R	5′-UGAUCUAACAACUUCAGUCTT-3′
5	siKIF14-3-F	5′-GCAAUGAUUGCUACGAUUATT-3′
6	siKIF14-3-R	5′-UAAUCGUAGCAAUCAUUGCTT-3′
7	SiCtrl-F	5′-UUUGUACUACACAAAAGUACUG-3′
8	SiCtrl-R	5′-CAGUACUUUUGUGUAGUACAAA-3′

Table 2 The gene primers sequences for qPCR analysis

Serial number	Primer name	Primer sequence (5′ to 3′)
1	GAPDH-F	5′-AGAAGGCTGGGGCTCATTTG-3′
2	GAPDH-R	5′-AGGGGCCATCCACAGTCTTC-3′
3	KIF14-F	5′-CCTCACCCACAGTAGCCGA-3′
4	KIF14-R	5′-AAGTGCCAATCTACCTACAGGA-3′
5	CyclinD1-F	5′-GCTGCGAAGTGGAAACCATC-3′
6	CyclinD1-R	5′-CCTCCTTCTGCACACATTTGAA-3
7	CDK4-F	5′-ATGGCTACCTCTCGATATGAGC-3′
8	CDK4-R	5′-CATTGGGGACTCTCACACTCT-3′

5% CO2. For siRNA transfection in A498 cells, we utilized both control (siCtrl) and KIF14-targeting siRNAs (siKIF14), and the transfection was performed using X-tremeGENE siRNA Transfection Reagent (Roche). The siRNA sequences were list as Table 1.

Western blotting assay

The A498 cells were subjected to lysis in RIPA buffer supplemented with protease inhibitors, followed by complete homogenization. Following centrifugation, the supernatant was collected, and the overall protein concentration was quantified using a BCA assay. Subsequently, the protein samples were denatured and separated by sodium dodecyl sulfate-polyacrylamide gel electrophoresis. The separated proteins were then transferred onto PVDF membranes, which were subsequently blocked using a 5% non-fat milk/TBST solution. After blocking, the membranes were treated with primary antibody solutions for one night at 4 °C. They were then washed three times with TBST. Next, the membranes were incubated with a secondary antibody solution. Finally, the membranes were washed with TBST three additional times and incubated with an ECL working solution. A Las-3000 Luminescent Image Analyzer (Fujifilm, Japan) was used to visualize the signals. The antibodies used for Western blotting are as follows: KIF14 antibody (1:1000, 26000-1-AP, Proteintech, China), GAPDH antibody (1:10000, 10494-1-AP, Proteintech, China), CyclinD1 antibody (1:5000, 60186-1-lg, Proteintech, China), CDK4 antibody (1:2000, 11026-1-AP, Proteintech, China), β-actin (1:10000, 11224-1-AP, Proteintech, China), and HRP-conjugated goat anti-rabbit IgG (1:10000, 511203/511103, ZENBIO, China).

qPCR assay

Following the protocol provided by the manufacturer, total RNA was isolated from A498 cells using TRIzol reagent (Invitrogen, USA). Then, cDNA was synthesized using the PrimeScript™ RT Master Mix (TAKARA, Japan). For qPCR, the TB Green Premix Ex Taq II (TAKARA, Japan) was employed, and the relative expression levels of KIF14 was calculated using the $2-\Delta\Delta Cq$ method. The primers used for qPCR analysis were list as Table 2.

Colony formation assay

Cells transfected with siCtrl or siKIF14 were seeded at a density of 600 cells per well in 6-well plates and grown for 11 days. Following that, the cells were washed with PBS and fixed for 30 min in 4% paraformaldehyde. After fixation, they were stained with 0.5% crystal violet for 15 min. After that, the cells were washed, and an IX73 inverted microscope (OLYMPUS, Japan) was used to take pictures of the colonies, which were then quantified using ImageJ software (NIH).

Cell proliferation assay

Cell proliferation was measured using the CCK-8 assay. Briefly, A498 cells were planted at an average density of 2,000 cells per well in 96-well plates. After 24 h, either control or KIF14-targeting siRNA was transfected into the cells. Following an additional 24-hour incubation, CCK-8 solution (C0037, Beyotime, China) was added to the 96-well plate on the 1st, 2nd, 3rd, 4th, and 5th day to measure cell proliferation. The OD450 values were determined using an Infinite F50 microplate reader (Tecan).

Cell cycle assay

To examine the cell cycle, A498 cells were seeded in 6-well plates at a density of 1×10^6 cells per well. After 24 h, the cells were transfected with either control or KIF14-targeting siRNA. Following an additional 24-hour incubation, the cells were treated with pre-chilled ethanol overnight at -20 °C. Subsequently, they were washed with PBS and incubated with a 7-AAD/PBS solution in the dark for 30 min at 4 °C. Finally, a BD FACSCanto™ II machine was used for flow cytometry analysis, and the results were processed with FlowJo software (v10).

Apoptosis assay

Following the manufacturer's instructions, the FITC Annexin V Apoptosis Detection Kit with propidium iodide (PI) (#640914, Biolegend) was used to detect apoptotic cells. In brief, A498 cells were seeded in 6-well plates at a density of 1×10^6 cells per well and cultured for 24 h. Subsequently, the cells were transfected with either siCtrl or siKIF14. After 24 h, the cells were washed with PBS, digested with a 0.25% trypsin solution, pelleted,

resuspended in Annexin V binding buffer, and treated with Annexin V-FITC/PI working solution. Finally, flow cytometry analysis was performed using a BD FACSCanto™ II machine, and the results were analyzed using FlowJo software (v10).

Statistical analysis

The differential expression of KIF14 was assessed using the Wilcoxon rank-sum test, ilcoxon signed rank test or Paired Sample t-Test. Overall survival (OS) was analyzed using the Kaplan–Meier method and the log-rank test. Correlation analysis was conducted using Spearman correlation analysis. Unpaired Student's t-tests and one-way ANOVA were employed for comparisons between two groups and multiple groups, respectively, utilizing GraphPad Prism (v8) or R software (version 4.1.0). All experimental results were presented as the mean ± SEM, with statistical significance set at $p < 0.05$. All experiments in this study were conducted in triplicate for the purpose of quantification.

Results

KIF14 expression is upregulated in ccRCC tissues

To evaluate the involvement of KIF14 in ccRCC, we used R software to explore the TCGA KIRC cohort to analyze whether KIF14 exhibits different expression levels of mRNA in clear cell renal cell carcinoma. The results revealed that the transcriptional levels of KIF14 was elevated in kidney cancer tissues compared with normal tissues (Figs. 1A and B and 530 tumors vs. 72 normals, $^{***}p < 0.001$). ROC curves were constructed to determine the diagnostic accuracy of KIF14 expression. As shown in Fig. 1C, the KIF14 expression had a high sensitivity and specificity for KIRC diagnosis. The area under the curve (AUC) was 0.928 (95%CI: 0.884–0.973). Subsequently, we analyzed the GSE15641 (Figs. 1D and 32 tumors vs. 23 normals, $^{***}p < 0.001$) and GSE40435 (Figs. 1E and 101 paired cohort, $^{***}p < 0.001$) dataset and E-MTAB-1805 (Figs. 1F and 105 tumors vs. 15 normals, $^{***}p < 0.001$) cohort data to confirm the expression difference of KIF14 between ccRCC samples and healthy tissues. It can be observed that the KIF14 is highly expressed in primary kidney tumors. Our preliminary studies demonstrated that KIF14 is a potential oncogene in clear cell renal cell carcinoma. Genetic perturbation similarity analysis with KIF14 in KIRC from the TCGA dataset were investigated. We compared 271 KIRC KIF14-high samples with 270 KIF14-low controls. A total of 674 differentially expressed genes (DEGs), covering 354 upregulated GENEs and 320 downregulated GENEs ($|LogFC| > 1$ & $p.adj < 0.05$) as shown in Fig. 1G. DESeq2 package was used to analyze DEGs in HTSeq-Counts. Figure 1H shows the relative expression levels of the top 10 DEGs between the two cohorts.

Analysis of the association between KIF14 expression and clinicopathological characteristics

In order to understand the role and significance of HTRA3 expression, 539 KIRC samples from the TCGA were analyzed for KIF14 expression data and all patient characteristics. As shown in Fig. 2A–E, high KIF14 was remarkably associated with T stage (T3 & T4 vs. T1 & T2, $^{***}P < 0.001$), clinical stage (stage III & stage IV vs. stage I & stage II, $^{***}P < 0.001$), histological grade (grade 3 & grade 4 vs. grade 1 & grade 2, $^{**}P < 0.01$), N stage (N1 vs. N0, $^{*}P < 0.05$), and M stage (M1 vs. M0, $^{***}P < 0.001$). Nevertheless, KIF14 expression has no relation with age (Fig. 2F). The univariate analysis using Logistic regression revealed that KIF14 expression as a categorical dependent variable was related with poor prognostic clinicopathological variables (Table 3). overexpressed HTTA3 expression in KIRC is positively correlated with T stage (OR = 2.27 for T3 & T4 vs. T1 & T2, 95%CI: 1.586–3.280), N stage (OR = 6.50 for N1 vs. N0, 95%CI: 1.765–41.941), M stage (OR = 2.53 for M1 vs. M0, 95%CI: 1.518–4.335), pathologic stage (OR = 2.15 for stage III & stage IV vs. stage I & stage II, 95%CI: 1.509–3.076) and histological grade (OR = 2.16 grade 3 & grade 4 vs. grade 1 & grade 2, 95%CI: 1.532–3.069). This turned out to be the KIRC with high KIF14 expression were more likely to progress to a more advanced stage compared to those with low kif14 expression.

Functional enrichment and analysis of KIF14-related signaling pathways

To delve into the biological pathways associated with KIF14 interactive genes in KIRC, we utilized GO and KEGG terms enrichment analysis employing the clusterProfiler R package. As depicted in Fig. 3A, genes related to KIF14 were implicated in various biological processes (BPs), cellular compositions (CCs), and molecular functions (MFs), including nuclear division, cell cycle checkpoint, chromosomal region, tubulin binding, among others. The KEGG analysis showed that the genes associated with KIF14 were strongly correlated with the Cell cycle, Human T-cell leukemia virus 1 infection, p53 signaling pathway, NOD-like receptor signaling pathway, and so on (Fig. 3B). We also validated the functional enrichment analysis of KIF14-related genes using the online analysis tool Metascape, and the results were highly consistent (Fig. S1). For the sake of determining KIF14-related signaling pathways in KIRC, GSEA was used to identify prominently activated signaling pathways between low and high KIF14 expression in KIRC, and their notable enrichment differences ($p.adjust < 0.05$ & $FDR < 0.25$) were validated in the Hallmark gene sets (MSigDB, h.all.v7.4.symbols.gmt). Based on their normalized enrichment score (HES), the most significantly enriched pathways were selected. This turned out to be

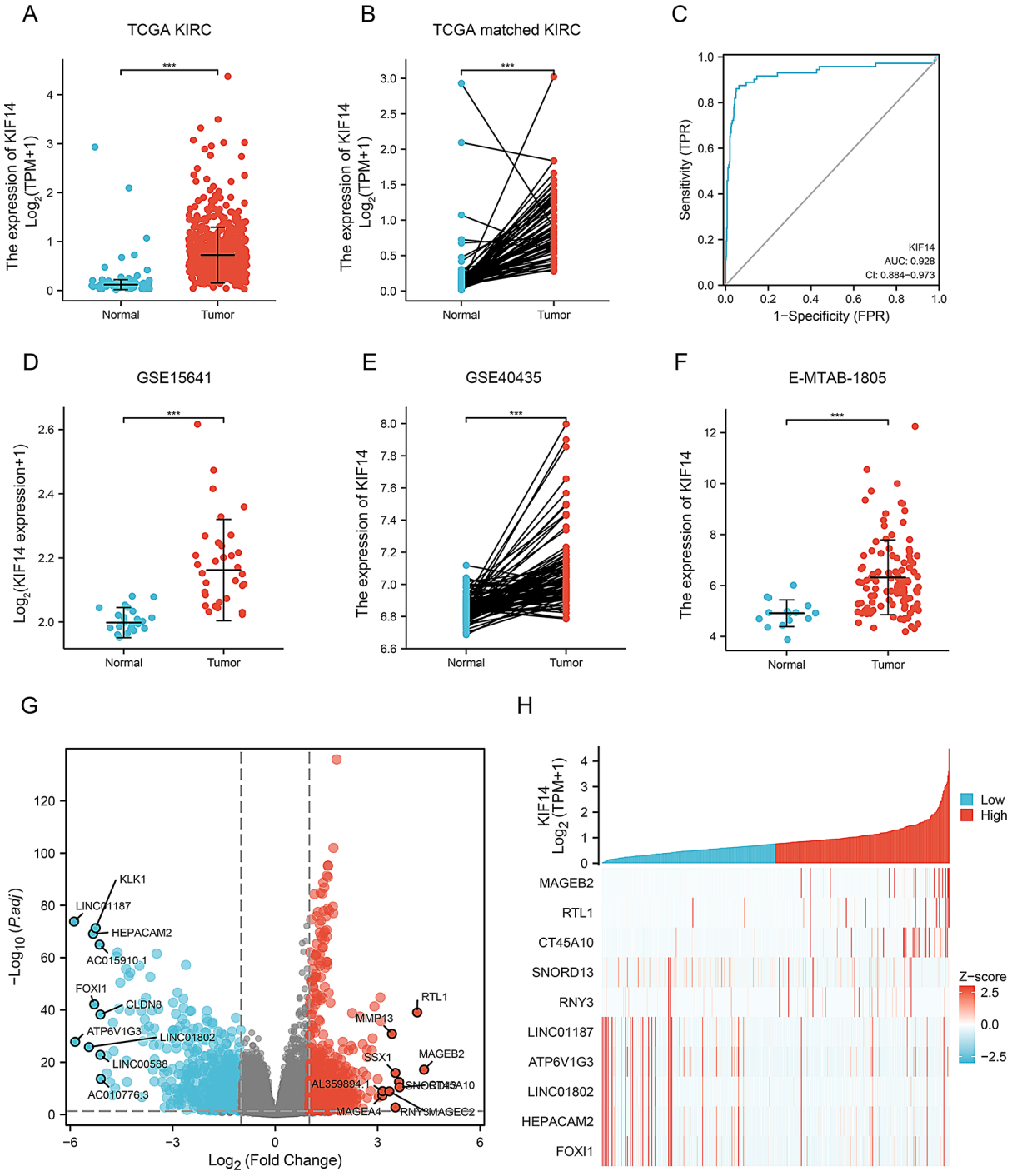

Fig. 1 Expression of KIF14 in kidney cancer. (**A**, **B**) Differential expression levels of KIF14 in TCGA-KIRC. (**C**) ROC curve of KIF14. (**D**, **E**) Differentially expressed KIF14 in normal tissue and ccRCC tissue from GSE15641 and GSE40435 database. (**F**) Differentially expressed KIF14 in normal tissue and ccRCC tissue from E-MTAB-1805 database. (**G**, **H**) Volcano plots of the DEGs and heat map showing the top 10 DEGs. *$p < 0.05$, ***$p < 0.001$. KIRC, kidney renal clear cell carcinoma; AUC, area under the curve

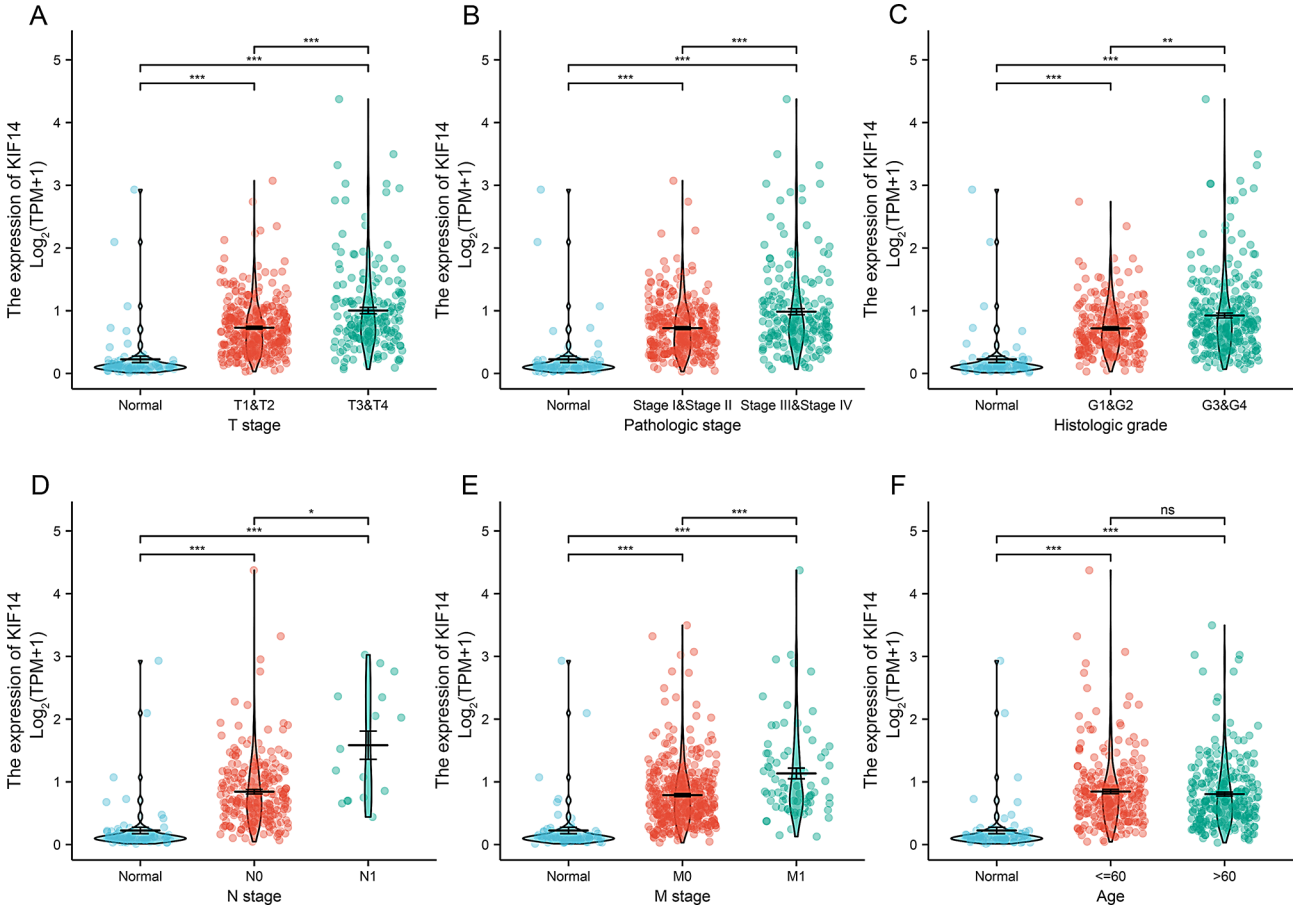

Fig. 2 Relationship between KIF14 expression and clinicopathological characteristics, including (**A**) T stage histological type, (**B**) pathologic stage, (**C**) histological grade, (**D**) N stage, (**E**) M stage, and (**F**) age in KIRC patients in TCGA cohort. *$p < 0.05$, **$p < 0.01$, ***$p < 0.001$

Table 3 KIF14 expression association with clinical pathological characteristics (logistic regression)

Characteristics	Total(*N*)	Odds Ratio(OR)	*P* value
T stage (T3&T4 vs. T1&T2)	539	2.274 (1.586–3.280)	< 0.001
N stage (N1 vs. N0)	257	6.496 (1.765–41.941)	0.015
M stage (M1 vs. M0)	506	2.529 (1.518–4.335)	< 0.001
Pathologic stage (Stage III & Stage IV vs. Stage I & Stage II)	536	2.149 (1.509–3.076)	< 0.001
Histologic grade (G3 & G4 vs. G1 & G2)	531	2.164 (1.532–3.069)	< 0.001
Primary therapy outcome (PD & SD& PR vs. CR)	147	0.704 (0.248–1.867)	0.489

the pathways that showed differential enrichment in the KIF14 high expression phenotype included G2M checkpoint, E2F targets, IL6 JAK STAT3 signaling, allograft rejection, interferon gamma response, and so on. In addition, pathways in the KIF14 low expression phenotype included oxidative phosphorylation, fatty acid metabolism, and adipogenesis (Fig. 3C).

Correlation analysis between KIF14 expression and immune cell infiltration in ccRCC

The results of functional enrichment analysis by appeal suggest that KIF14 may be involved in immune cell infiltration or immune checkpoints in RCC. Therefore, we performed immune infiltration analysis by both ssGSEA and CIBERSORT in TCGA KIRC patients. As shown in Fig. 4A and B, the expression of KIF14 was positively associated with helper T2 (Th2) cells, T helper cells, Macrophages, Treg, Tcm, B cells, etc. and negatively associated with the NK cells, helper T17 (Th17) cells, and pDC. Furthermore, CIBERSORT analysis exposed the expression of KIF14 was negatively associated with Mast cells resting, Dendritic cells activated, NK cells activated, etc. and positively associated with T cells CD4 memory activated, and Macrophages M1 (Fig. 4C and D). The tumor microenvironment comprises a complex interplay of stromal cells, tumor cells, and immune cells. Stromal cells play a supportive role in tumor growth, while immune cells can either promote or inhibit tumor growth. To gain a deeper understanding of the relevance and underlying mechanism of KIF14 expression in ccRCC, we assessed

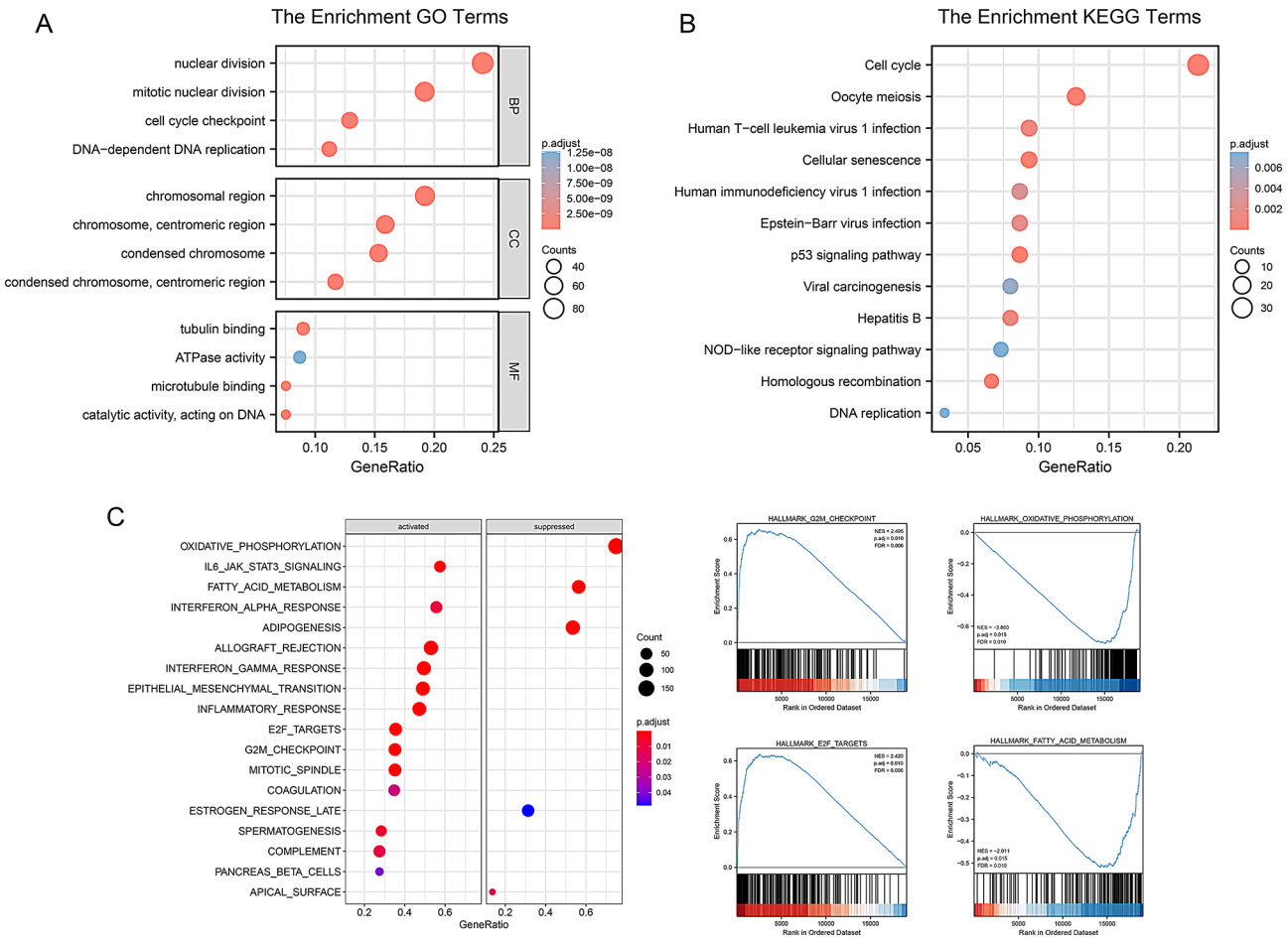

Fig. 3 Functional and pathway enrichment analysis of KIF14-related genes in KIRC. (**A**) GO terms enrichment analysis. (**B**) KEGG pathway enrichment analysis. (**C**) GSEA analysis for KIF14 between low and high expression in KIRC. BP, biological processes; CC, cellular compositions; MF, molecular functions; NES, normalized enrichment score; *p*.adj, adjusted *P* value; FDR, false discovery rate

the relationship between immune and stromal scores and KIF14 expression using ESTIMATE analysis. KIF14 expression exhibited a positive correlation with tumor immune, stromal and ESTIMATE scores (sum of immune scores and stromal scores), and the group with a low level of KIF14 expression had a lower abundance of stromal cells and immune cells than the group with a higher level of KIF14 expression (Fig. 4E-J, $^{***}p < 0.001$). Secondly, we examined the potential efficacy of immunotherapy in low and high KIF14 expression groups using TIDE analysis (Fig. 4K, $^{*}p < 0.05$, $^{***}p < 0.001$). The KIF14-high group The KIF14-high group had higher TIDE, T-cell dysfunction scores, suggesting that immune escape may be more likely to occur in KIF14-high patients. Moreover, KIF14 expression was inversely correlated with tumor purity and positively correlated with cancer-associated fibroblasts (CAF) (Fig. 4L).

Elevated KIF14 expression was intimately correlated with poor prognosis of patients with KIRC

As shown in Fig. 5A, among KIRC patients with low KIF14 expression, the 10-year OS rate was remarkably higher than those with high HTRA3 expression (47.2 vs. 39.7%, HR = 1.422, $p = 0.020$, 95%CI: 1.057–1.913). Likewise, the 10-year DSS rates and PFI were appreciably higher in the KIF14 low group than in the KIF14 high group (66.9 vs. 60.2%; $p = 0.002$, 95%CI: 1.245–2.639; 55.6 vs. 37.5%; $p = 0.001$, 95%CI: 1.216–2.261; Fig. 5B, C). We then performed subgroup survival analyses for OS, DSS and PFI. The results showed a poorer prognosis in patients with high KIF14 expression in the stage III-IV, stage IV and M1 subgroups for OS and in the grade 3 & 4, T3 & T4 and M1 subgroups for DSS (Fig. 5D-I). In addition, KIRC patients with high KIF14 levels in the M1 subgroup had worse OS and DSS rates (15.3 vs. 4.0%; $p = 0.021$; 16.7 vs. 4.3%; $p = 0.020$, 95%CI: 1.074–2.883), suggesting that KIF14 has a greater prognostic role in KIRC patients with distant metastases. However, there

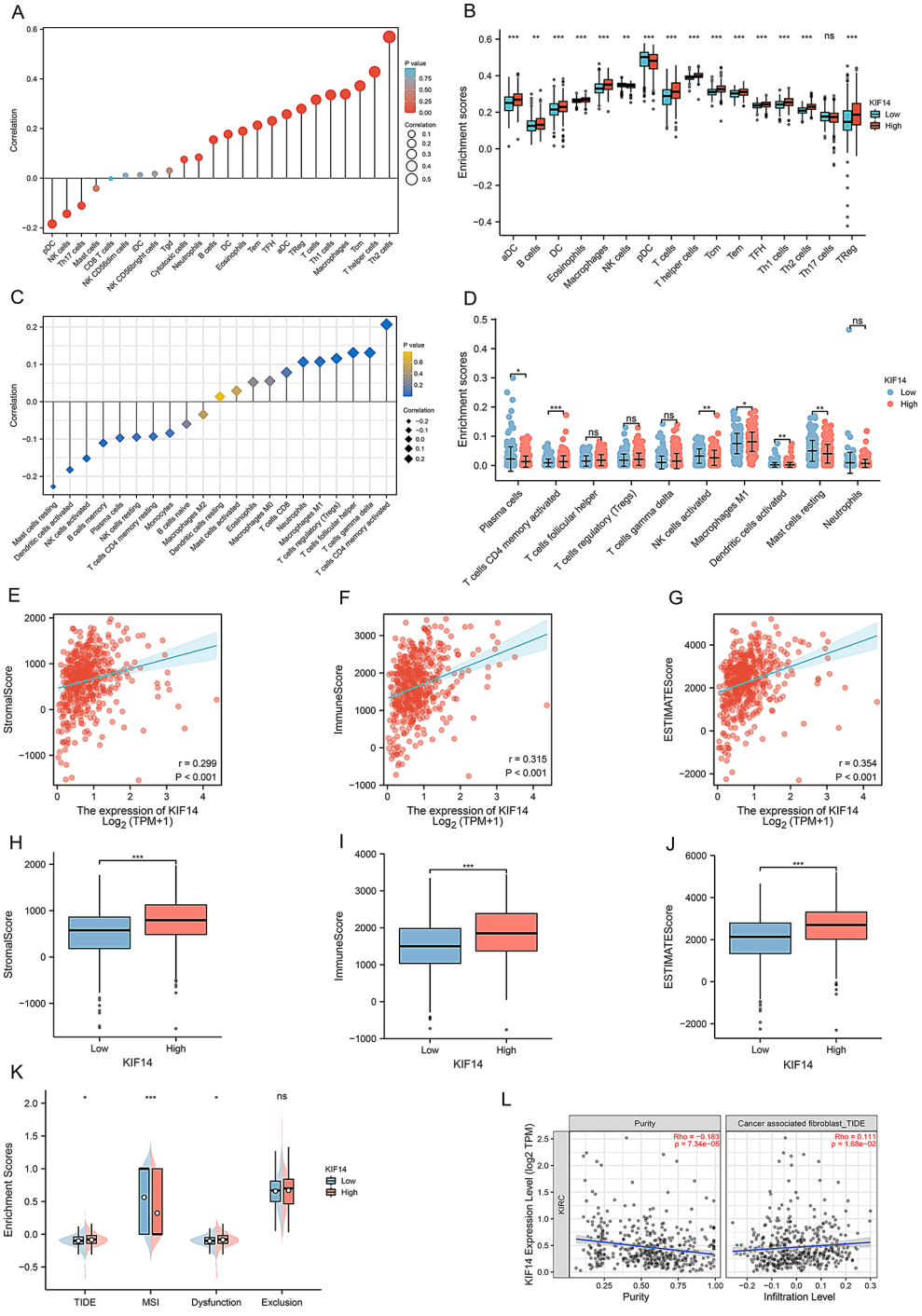

Fig. 4 KIF14 expression was associated with the immunocytes infiltration and response to immunotherapy in ccRCC. (**A**) The correlation between the expression of KIF14 and the relative abundance of 24 immune cells was analyzed by ssGSEA. (**B**) The difference in the infiltration level of 16 immune cells between the KIF14 high and low groups. (**C**) The correlation between the expression of KIF14 and the relative abundance of 21 immune cells was analyzed by CIBERSORT. (**D**) The difference in the infiltration level of 10 immune cells between the KIF14 high and low groups. (**F**-**H**) The relationship between tumor immune/stromal/ESTIMATE scores and KIF14 expression levels. (**I**-**K**) The difference in tumor immune/stromal/ESTIMATE scores between the KIF14 high and low groups. (**L**) TIDE, MSI, T cell dysfunction and Exclusion scores in the KIF14 high and low groups. (**M**) The correlation between tumor purity/CAF and KIF14 expression levels. TIDE, Tumor Immune Dysfunction and Exclusion; MSI, microsatellite instability; CAF, cancer-associated fibroblasts. *$p < 0.05$, **$p < 0.01$, ***$p < 0.001$

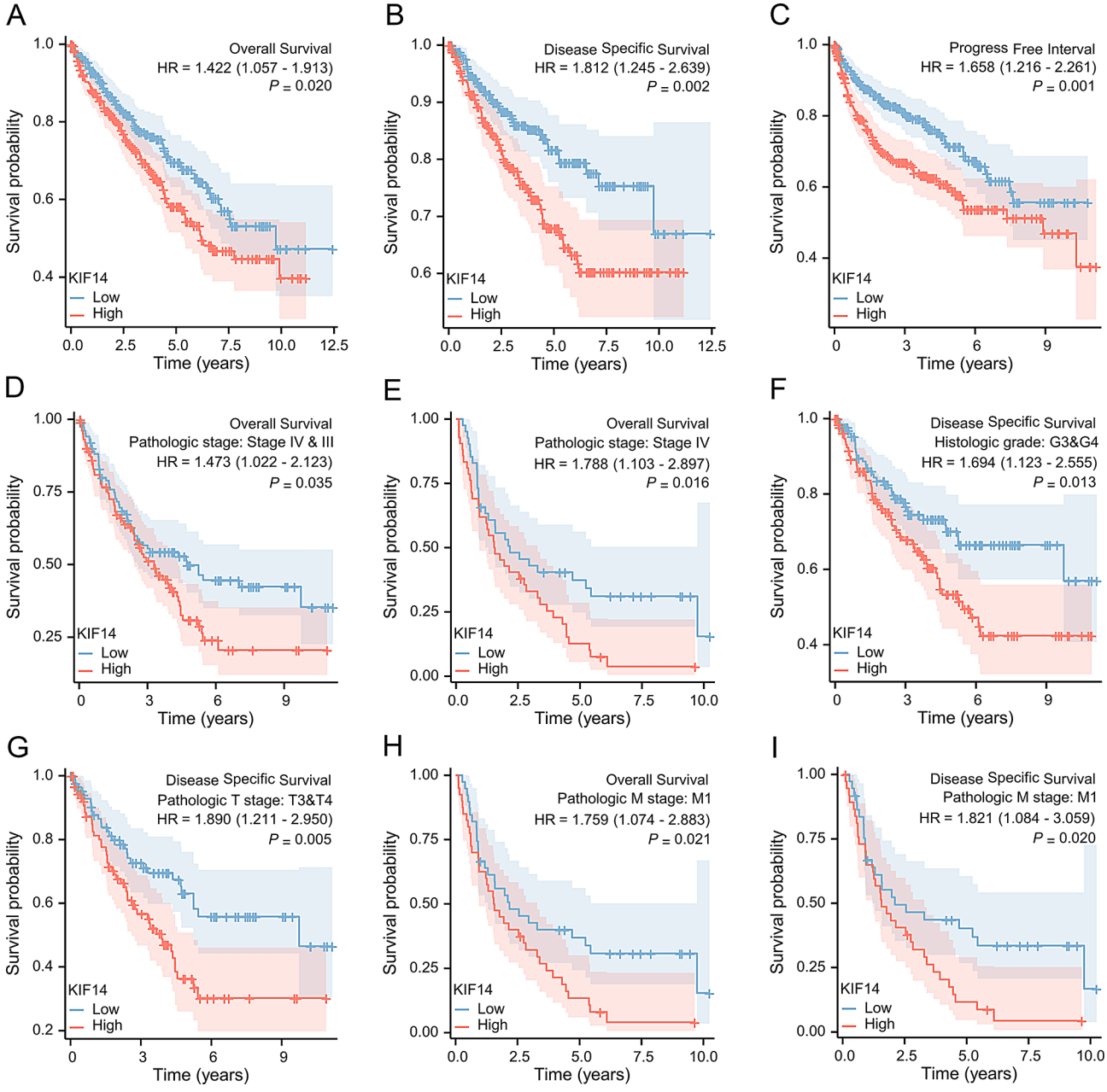

Fig. 5 Kaplan–Meier overall survival curve for high and low KIF14 expression in KIRC. (**A**-**C**) Survival curves showing OS, DSS and PFI comparing patients with high and low levels of KIF14 in KIRC. (**D**, **E**, **H**) Survival curves showing OS with stage III & IV, stage IV, and MI subgroups. (**F**, **G**, **I**) DSS survival curves of grade3 & 4, T3 & T4, and MI subgroups. KIRC, kidney renal clear cell carcinoma; OS, overall survival; DSS, disease specific survival; PFI, progression free interval

was no significant difference in survival between the PFI subgroups.

Dysregulation of KIF14 expression may be mediated by the miR-200b/200a/429 cluster in ccRCC

Many previous studies have shown the presence of a large number of dysregulated microRNAs (miRNAs) in ccRCC, and miRNAs bind to the 3'UTR region of mRNAs and inhibit post-transcriptional translation of mRNAs. To investigate whether miRNAs are involved in the mechanism of dysregulation of KIF14 overexpression in ccRCC, we examined the relevant miRNAs leading to KIF14 overexpression using microT-CDS v5.0 [30]. An interesting finding was that there was a regulatory relationship between KIF14 and the miR-200b/200a/429 cluster (Fig. 6A and D). Next, we found that hsa-miR-429 and has-miR-200b-3p were low expressed in tumor compared to the normal groups and inversely correlated with

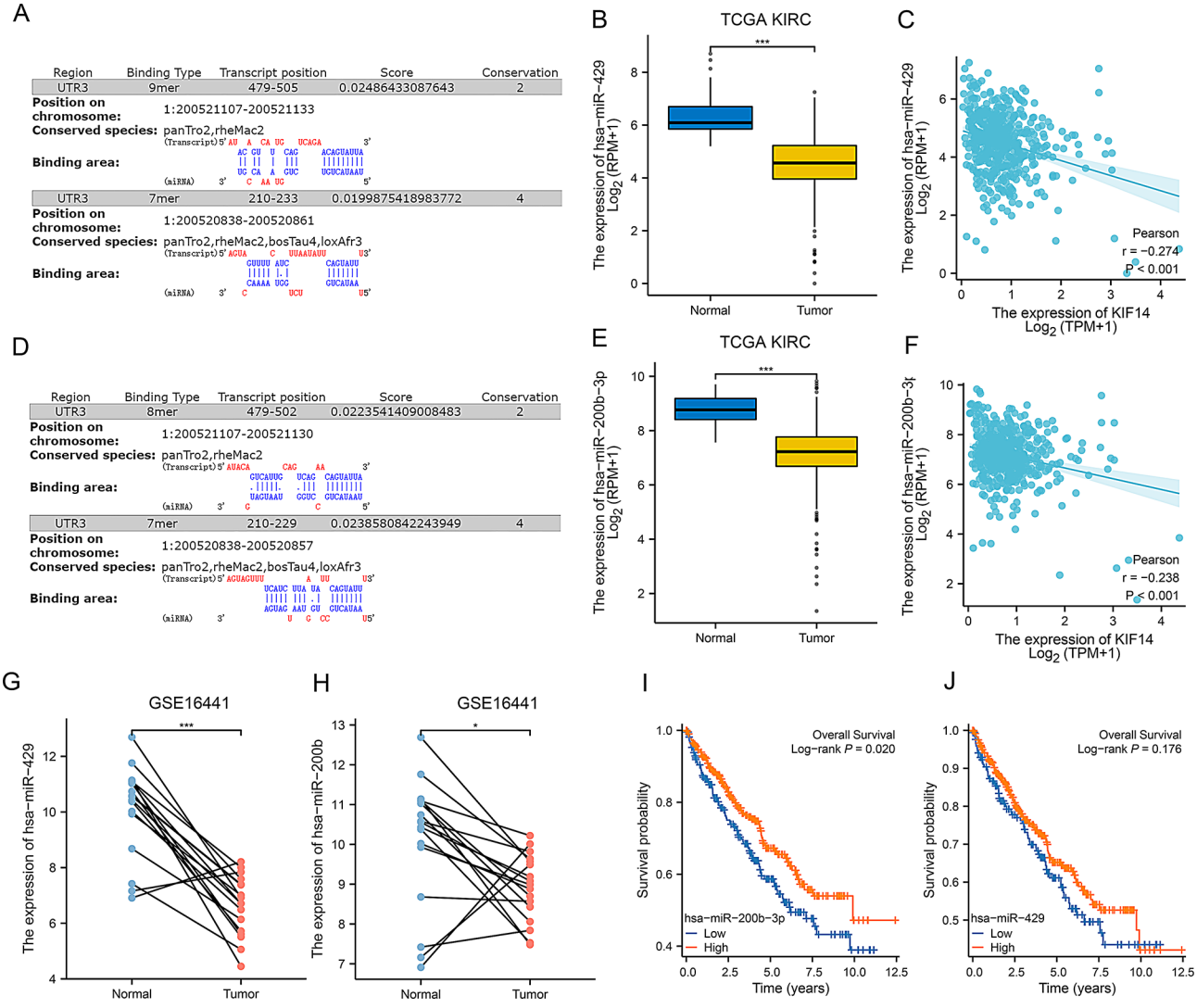

Fig. 6 The miR-200b/200a/429 cluster leads to upregulation of KIF14 expression in ccRCC. (**A**, **D**) Possible hsa-miR-429 and has-miR-200b-3p binding sites for KIF14. (**B**, **E**) Differentially expressed hsa-miR-429 and has-miR-200b-3p in normal tissue and ccRCC tissue from TCGA KIRC database. (**C**, **F**) Correlation analysis between hsa-miR-429/has-miR-200b-3p and KIF14. (**G**, **H**) Analysis of paired differential expression of hsa-miR-429 and has-miR-200b-3p from GSE16441. (**I**, **J**) Kaplan-Meier analysis of overall survival was analyzed according to hsa-miR-429 and has-miR-200b-3p expression levels. $^{*}p < 0.05$, $^{**}p < 0.01$, $^{***}p < 0.001$

KIF14 expression in the TCGA KIRC cohort (Fig. 6B, C, E and F, $^{***}p < 0.001$). The GSE16441 dataset was analyzed to further validate that hsa-miR-429 and has-miR-200b-3p were poorly expressed in tumors (Fig. 6G and H). Although there were no statistically significant differences in OS between the low and high hsa-miR-429 expression groups, we observed that patients in the high miR-200b-3p expression group had a better prognosis (Fig. 6I, $p = 0.020$, 95%CI: 0.522–0.947).

KIF14 knockdown reduced proliferation, attenuated colony-forming ability, impaired cell cycle and increased apoptosis of A498 ccRCC cells

We detected and compared the differences in mRNA levels of KIF14 in normal kidney cells and three different renal clear cell carcinoma cell lines by qPCR, respectively, and through the experimental results, we found that KIF14 expression was up-regulated in renal clear cell carcinoma cells and identified A498 as a renal clear cell carcinoma cell line with high expression of KIF14 (Fig. 7A). To investigate the function of KIF14 in ccRCC, we initially depleted KIF14 in A498 cells. qPCR and Western blotting confirmed that all three siRNAs targeting KIF14 efficiently reduced KIF14 expression in A498 cells, with siKIF14-1 showing the highest knockdown efficiency (Fig. 7B-C). Therefore, we selected siKIF14-1 (hereafter referred to as siKIF14) for subsequent experiments. A CCK8 test was performed to evaluate the effect of KIF14 knockdown on the proliferation of A498 cells, which revealed a significant decrease in proliferation

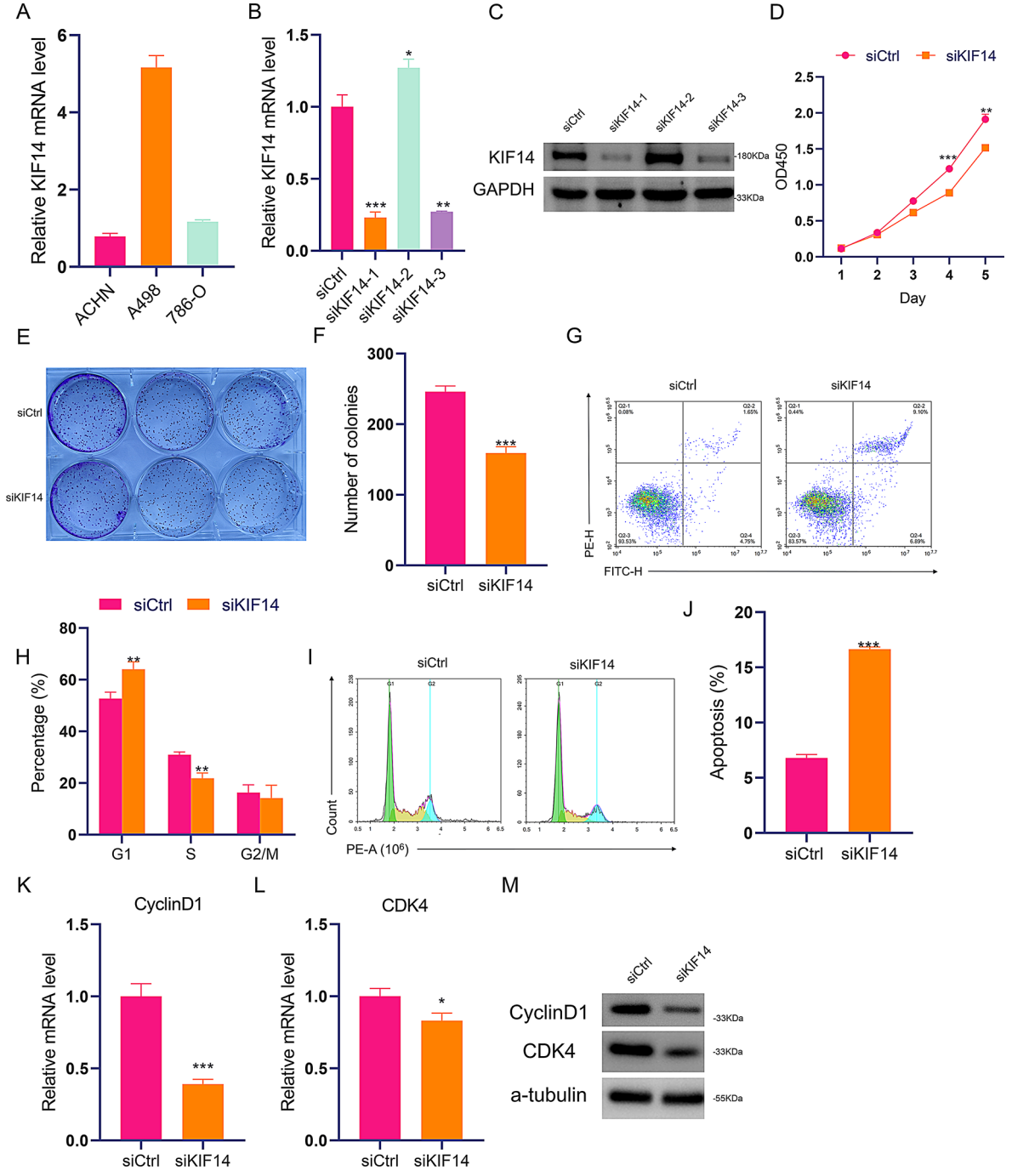

Fig. 7 The effect of KIF14 deficiency on A498 cells. (**A**) qPCR revealing higher KIF14 mRNA expression in ACHN, A498 and 786-0 compared to HKC. (**B**) qPCR analysis results showing the downregulation of KIF14 expression in A498 cells by three different siRNAs targeting KIF14. (**C**) Western blotting data confirming the significant decrease in KIF14 expression in A498 cells upon siRNA-mediated knockdown. (**D**) CCK8 assay results indicating reduced proliferation of KIF14-deficient A498 cells compared to control A498 cells. (**E**) Colony formation assay showing attenuated colony expansion capacity in A498 cells following KIF14 depletion. (**F**) Quantification of the colony formation assay results presented in (**E**). (**G**) 7-AAD staining data demonstrating cell cycle arrest in A498 cells upon KIF14 depletion. (**H**) Quantification of the cell cycle analysis results shown in (**G**). (**I**) Annexin V/PI staining outcomes revealing increased apoptosis in KIF14-depleted A498 cells. (**J**) Quantification of the apoptosis analysis results presented in (**I**). (**K**, **L**) qPCR analysis results demonstrating that CDK4 and CyclinD1 mRNA expression levels were downregulated in KIF14-deficient A498 cells compared to normal cells. (**M**) The level of CDK4 and CyclinD1 were detected by Western blotting. CyclinD1, CCND1. *$p < 0.05$, **$p < 0.01$, ***$p < 0.001$

in KIF14-deficient A498 cells compared to control cells (Fig. 7D). The data obtained from the colony formation assay provided additional evidence that the absence of KIF14 significantly compromised the ability of A498 cells to generate colonies (Fig. 7E and F). Consistent with these findings, KIF14 depletion led to cell cycle arrest and an increased level of apoptosis in A498 cells, as indicated by 7-AAD and Annexin-V/PI staining results (Fig. 7G-J). Furthermore, through the pre-functional enrichment analysis, we found that KIF14 was strongly associated with the cell cycle as shown in Fig. 3. Therefore, we examined the expression levels of CDK4 and CyclinD1 (CCND1) in KIF14-deficient A498 cells by qPCR, and the results were as we expected, the expression levels of both CDK4 and CyclinD1 were decreased after reduced KIF14 expression in A498 cells (Fig. 7K-M). Spearman correlation analysis also showed that KIF14 expression was positively correlated with CDK4 and cyclinD1 in the TCGA KIRC cohort (Fig. S2). Taken together, these observations provide strong evidence for the oncogenic role of KIF14 in ccRCC.

Discussion

Numerous literature reports have indicated that KIF14 demonstrates oncogenic properties in various malignant tumors; however, its involvement in the pathogenesis of clear cell renal cell carcinoma (ccRCC) has been minimally addressed in the literature. Therefore, this study sought to investigate the potential role of KIF14 in ccRCC. Initial bioinformatic analysis utilizing public databases revealed that KIF14 expression is significantly upregulated and serves as a diagnostic marker in ccRCC. Subsequent investigations demonstrated that elevated KIF14 expression in ccRCC is correlated with advanced clinicopathological characteristics, alterations in the cell cycle, immune infiltration, immune evasion, reduced survival rates and poorer prognosis. Finally, it has been shown experimentally that inhibition of KIF14 expression in A498 cells suppresses cell proliferation and renders the cells more susceptible to apoptosis. All this suggests that KIF14 may be a potential prognostic marker for ccRCC patients.

KIF14 is a member of the N-type, kinesin 3 superfamily located on chromosome 1q32.1 and is required for cellular chromosome segregation and cytokinesis processes [11, 12, 31]. KIF14 is overexpressed in a variety of cancers, including gastric [32], hepatocellular [33], colorectal [15], and cervical [18], and is strongly associated with poor prognosis. Consistent with this, our data showed that KIF14 was highly expressed in ccRCC tissues (shown in Fig. 1A-B and D-F) and kidney cancer cells (shown in Fig. 7A) and that KIF14 overexpression significantly correlated with pathologic stage, histological grade, T stage and M stage of RCC (shown in Fig. 2). The higher KIF14 expression in patients with ccRCC, the worse histological types, lower tumor differentiation, later clinicopathological stages, and poorer prognosis (shown in Fig. 5), further supporting the idea of KIF14 as an oncogene, and experimental validation showed that knockdown of KIF14 reduced proliferation, decreased colony-forming ability, impaired cell cycle and increased apoptosis in A498 ccRCC cells (shown in Fig. 7D-J). Although METL14 in combination with KIF14 has better diagnostic potential [34], our results showed that KIF14 also had better diagnostic potential in ccRCC (shown in Fig. 1C). FOXI1 acts as a biomarker for renal intercalated cell (IC)-associated tumors and can partially reprogram the ccRCC cell line 786-O towards the transcriptional phenotype of chromophobe renal cell carcinoma (chRCC) [35, 36]. Interestingly, genetic perturbation similarity analysis with KIF14 in KIRC showed a biological link between FOXI1 and KIF14 (shown in Fig. 1G-H), but further relevant experiments are needed to verify this.

KEGG pathway analysis implicated that KIF14 is involved in cell cycle regulation, and low levels of CDK4 and cyclinD1 in KIF14-deficient A498 cells compared to control cells were confirmed in subsequent experimental studies (shown in Fig. 7K-L). In addition, we also showed that the KIF14-high phenotype was correlated with the G2/M checkpoint signaling pathway, p53 signaling pathway, E2F targets, IL6/JAK/STAT3 and the KIF14-low phenotype was correlated with the oxidative phosphorylation, fatty acid metabolism (shown in Fig. 3C). Recent studies have shown that maintenance of the G2/M checkpoint influences the effects of immunotherapy response in kidney cancer [37], and in a study of 103 patients with untreated clear cell renal cell carcinoma, downregulation of oxidative phosphorylation-related metabolism was among the many pathways dysregulated in ccRCC [38]. Here, Du et al. found that abnormal fatty acid metabolism in ccRCC leads to activation of lipid storage pathways as a necessary step in the development of malignancy [39]. This demonstrates that KIF14 may promote ccRCC cell growth, metastasis and poor survival through G2/M checkpoint or tumor metabolism signaling.

Li et al. identified the associations between 22 types of tumor infiltrated immune cells and clinical outcomes in ccRCC through bioinformatics analysis [40]. Our immune infiltration analysis revealed that KIF14-high tumors exhibit an immunosuppressive TME characterized by enriched Tregs and M1 macrophages, alongside depleted cytotoxic NK cells and dendritic cells (DCs) (Fig. 4A-D). This aligns with prior studies showing that Tregs suppress antitumor immunity by inhibiting effector T-cell activation [41]. while tumor-associated macrophages (TAMs) promote angiogenesis and extracellular matrix remodeling [42]. Notably, DCs are critical for antigen presentation and T-cell priming [43]; their reduction

in KIF14-high tumors may impair immune surveillance, facilitating immune escape. Mechanistically, we propose that KIF14-driven cell cycle dysregulation (via CyclinD1/CDK4 downregulation upon KIF14 knockdown; Fig. 7K-M) may indirectly shape the TME. Rapidly proliferating tumor cells (due to KIF14 overexpression) could alter metabolic demands (e.g., hypoxia, lactate accumulation), which recruit immunosuppressive cells like Tregs and M1-like macrophages [44, 45]. Supporting this, our GSEA indicated that KIF14-high tumors downregulate oxidative phosphorylation (Fig. 3C), a metabolic pathway linked to immune evasion in ccRCC. Our analysis further revealed that KIF14 expression positively correlated with ImmuneScore, StromalScore, and ESTIMATEScore, while inversely associated with tumor purity (Fig. 4E-J, L). These findings suggest that KIF14-high tumors harbor a more complex tumor microenvironment (TME) enriched with both immune and stromal components. The negative correlation between KIF14 and tumor purity underscores that KIF14-driven tumors are less dominated by malignant cells but instead infiltrated by diverse stromal and immune populations. This is consistent with studies showing that low tumor purity correlates with poor prognosis in cancers like gastric carcinoma [46], as non-tumor cells (e.g., cancer-associated fibroblasts, immune cells) can facilitate therapeutic resistance [47]. Clinically, the elevated TIDE score in KIF14-high patients (Fig. 4K) suggests heightened T-cell dysfunction, potentially explaining their poor response to immunotherapy. This is critical, as PD-1/PD-L1 inhibitors rely on pre-existing T-cell infiltration [48]. Future studies should explore whether KIF14 inhibition could synergize with immune checkpoint blockade by reversing TME suppression.

While our findings provide novel insights into KIF14's role in ccRCC, several limitations must be acknowledged. First, our analyses primarily relied on retrospective public datasets (e.g., TCGA, GEO), which may introduce selection bias due to heterogeneous clinical protocols or incomplete follow-up data. Second, the lack of in vivo validation (e.g., xenograft models) limits our ability to conclusively establish KIF14's oncogenic function in a physiological context. Third, while we identified correlations between KIF14 and immune infiltration, the causative mechanisms (e.g., whether KIF14 directly recruits Tregs or alters cytokine secretion) remain speculative. To address these gaps, future studies should: (1) validate KIF14's role in vivo using patient-derived xenografts (PDX) or genetically engineered mouse models (GEMMs) to recapitulate ccRCC progression and therapy resistance; (2) integrate multi-omics approaches (e.g., single-cell RNA-seq, spatial transcriptomics) to dissect how KIF14 reshapes the tumor-stroma-immune ecosystem; (3) explore clinical relevance by correlating KIF14 expression with immunotherapy response in prospective ccRCC cohorts; and (4) investigate therapeutic synergy between KIF14 inhibition (e.g., siRNA, small-molecule inhibitors) and immune checkpoint blockade. These efforts could bridge the translational gap and position KIF14 as an actionable target for precision oncology in ccRCC.

Conclusion

This study initially identified an upregulation of KIF14 expression in patients with ccRCC, with high expression levels correlating with disease progression, poor prognosis, and increased immune infiltration in ccRCC. Subsequent experiments demonstrated that knockdown of KIF14 in A498 cells led to reduced proliferation, decreased colony formation capacity, cell cycle arrest, increased apoptosis, and downregulation of CyclinD1 and CDK4. In conclusion, these results emphasize the overexpression and oncogenic function of KIF14 in ccRCC, suggesting that KIF14 may serve as a potential therapeutic target for the treatment of this disease.

Abbreviations

ccRCC	Clear cell Renal Cell Carcinoma
ROC	Receiver Operating Characteristic
GO	Gene Ontology
KEGG	Kyoto Encyclopedia of Genes and Genomes
GSEA	Gene Set Enrichment Analysis
ssGSEA	single-sample GSEA
TIDE	Tumor Immune Dysfunction and Exclusion
BPs	Biological Processes
CCs	Cellular Compositions
MFs	Molecular Functions

Supplementary Information

The online version contains supplementary material available at https://doi.org/10.1186/s12894-025-01732-8.

Supplementary Material 1: Supplementary Figure 1. Enrichment analysis via Metascape.

Supplementary Material 2: Supplementary Figure 2. Correlation analysis between CDK4/cyclinD1 and KIF14.

Supplementary Material 3

Supplementary Material 4

Supplementary Material 5

Acknowledgements

Not applicable.

Author contributions

Jie Wang and Xuejia Lai contributed to the conception and design of the research and performed the research, data analysis, and drafted the manuscript. Bi Li contributed to the data analysis. Sike Feng performed the research. Zhijun Sun contributed to the design of the study. HZ contributed to the design of the study and revised the manuscript. All authors read and approved the final manuscript.

Funding

Acknowledgements this work was supported by the Medical Science and Technology Project of Zhejiang Province (2023RC267).

Data availability
The datasets used and/or analysed during the current study are available from the corresponding author on reasonable request.

Declarations

Ethics approval and consent to participate
Data collections and processions were performed according to policies of GEO, ArrayExpress and TCGA project.

Consent for publication
Not applicable.

Competing interests
The authors declare no competing interests.

Received: 17 April 2024 / Accepted: 3 March 2025
Published online: 04 April 2025

References

1. Rini BI, Campbell SC, Escudier B. Renal cell carcinoma. Lancet. 2009;373(9669):1119–32.
2. Sung H, Ferlay J, Siegel RL, Laversanne M, Soerjomataram I, Jemal A, Bray F. Global Cancer statistics 2020: GLOBOCAN estimates of incidence and mortality worldwide for 36 cancers in 185 countries. CA Cancer J Clin. 2021;71(3):209–49.
3. Bukavina L, Bensalah K, Bray F, Carlo M, Challacombe B, Karam J, Kassouf W, Mitchell T, Montironi R, O'Brien T et al. Epidemiology of renal cell carcinoma: 2022 update. Eur Urol 2022.
4. Shuch B, Amin A, Armstrong AJ, Eble JN, Ficarra V, Lopez-Beltran A, Martignoni G, Rini BI, Kutikov A. Understanding pathologic variants of renal cell carcinoma: distilling therapeutic opportunities from biologic complexity. Eur Urol. 2015;67(1):85–97.
5. Kotecha RR, Motzer RJ, Voss MH. Towards individualized therapy for metastatic renal cell carcinoma. Nat Rev Clin Oncol. 2019;16(10):621–33.
6. Hu SL, Chang A, Perazella MA, Okusa MD, Jaimes EA, Weiss RH. The nephrologist's tumor: basic biology and management of renal cell carcinoma. J Am Soc Nephrol. 2016;27(8):2227–37.
7. Raghubar AM, Roberts MJ, Wood S, Healy HG, Kassianos AJ, Mallett AJ. Cellular milieu in clear cell renal cell carcinoma. Front Oncol. 2022;12:943583.
8. Jonasch E, Walker CL, Rathmell WK. Clear cell renal cell carcinoma ontogeny and mechanisms of lethality. Nat Rev Nephrol. 2021;17(4):245–61.
9. Miki H, Okada Y, Hirokawa N. Analysis of the Kinesin superfamily: insights into structure and function. Trends Cell Biol. 2005;15(9):467–76.
10. Hirokawa N, Tanaka Y. Kinesin superfamily proteins (KIFs): various functions and their relevance for important phenomena in life and diseases. Exp Cell Res. 2015;334(1):16–25.
11. Zhernov I, Diez S, Braun M, Lansky Z. Intrinsically disordered domain of Kinesin-3 Kif14 enables unique functional diversity. Curr Biol. 2020;30(17):3342–e33513345.
12. Corson TW, Huang A, Tsao MS, Gallie BL. KIF14 is a candidate oncogene in the 1q minimal region of genomic gain in multiple cancers. Oncogene. 2005;24(30):4741–53.
13. Zhong M, Gong L, Li N, Guan H, Gong K, Zhong Y, Zhu E, Wang X, Jiang S, Li J, et al. Pan-cancer analysis of Kinesin family members with potential implications in prognosis and immunological role in human cancer. Front Oncol. 2023;13:1179897.
14. Jin T, Ding L, Chen J, Zou X, Xu T, Xuan Z, Wang S, Chen J, Wang W, Zhu C, et al. BUB1/KIF14 complex promotes anaplastic thyroid carcinoma progression by inducing chromosome instability. J Cell Mol Med. 2024;28(7):e18182.
15. Ji J, Fu J. MiR-17-3p facilitates aggressive cell phenotypes in Colon cancer by targeting PLCD1 through affecting KIF14. Appl Biochem Biotechnol. 2023;195(3):1723–35.
16. Meng F, Zhang Z. MicroRNA-152 specifically targets Kinesin family member 14 to suppress the advancement of bladder cancer cells via PI3K/AKT pathway. Biochem Biophys Res Commun. 2024;692:149337.
17. Liu L, Li M, Zhang J, Xu D, Guo Y, Zhang H, Cang S. KIF14 mediates cabazitaxel-docetaxel cross-resistance in advanced prostate cancer by promoting AKT phosphorylation. Arch Biochem Biophys. 2023;737:109551.
18. Zhang J, Buranjiang G, Mutalifu Z, Jin H, Yao L. KIF14 affects cell cycle arrest and cell viability in cervical cancer by regulating the p27(Kip1) pathway. World J Surg Oncol. 2022;20(1):125.
19. Xu H, Choe C, Shin SH, Park SW, Kim HS, Jung SH, Yim SH, Kim TM, Chung YJ. Silencing of KIF14 interferes with cell cycle progression and cytokinesis by blocking the p27(Kip1) ubiquitination pathway in hepatocellular carcinoma. Exp Mol Med. 2014;46(5):e97.
20. Krus I, Brynychová V, Hlaváč V, Václavíková R, Kováčová M, Koževnikovová R, Kopečková K, Tornikidis J, Vrána D, Gatěk J, Souček P. Single nucleotide variants in KIF14 gene May have prognostic value in breast Cancer. Mol Diagn Ther. 2022;26(6):665–78.
21. Zhang Y, Narayanan SP, Mannan R, Raskind G, Wang X, Vats P, Su F, Hosseini N, Cao X, Kumar-Sinha C et al. Single-cell analyses of renal cell cancers reveal insights into tumor microenvironment, cell of origin, and therapy response. *Proc Natl Acad Sci U S A* 2021, 118(24).
22. Liu J, Lichtenberg T, Hoadley KA, Poisson LM, Lazar AJ, Cherniack AD, Kovatich AJ, Benz CC, Levine DA, Lee AV et al. An integrated TCGA Pan-Cancer clinical data resource to drive High-Quality survival outcome analytics. Cell 2018, 173(2).
23. Yu G, Wang L-G, Han Y, He Q-Y. ClusterProfiler: an R package for comparing biological themes among gene clusters. OMICS. 2012;16(5):284–7.
24. Zhou Y, Zhou B, Pache L, Chang M, Khodabakhshi AH, Tanaseichuk O, Benner C, Chanda SK. Metascape provides a biologist-oriented resource for the analysis of systems-level datasets. Nat Commun. 2019;10(1):1523.
25. Subramanian A, Tamayo P, Mootha VK, Mukherjee S, Ebert BL, Gillette MA, Paulovich A, Pomeroy SL, Golub TR, Lander ES, Mesirov JP. Gene set enrichment analysis: a knowledge-based approach for interpreting genome-wide expression profiles. Proc Natl Acad Sci U S A. 2005;102(43):15545–50.
26. Newman AM, Liu CL, Green MR, Gentles AJ, Feng W, Xu Y, Hoang CD, Diehn M, Alizadeh AA. Robust enumeration of cell subsets from tissue expression profiles. Nat Methods. 2015;12(5):453–7.
27. Hänzelmann S, Castelo R, Guinney J. GSVA: gene set variation analysis for microarray and RNA-seq data. BMC Bioinformatics. 2013;14:7.
28. Bindea G, Mlecnik B, Tosolini M, Kirilovsky A, Waldner M, Obenauf AC, Angell H, Fredriksen T, Lafontaine L, Berger A, et al. Spatiotemporal dynamics of intratumoral immune cells reveal the immune landscape in human cancer. Immunity. 2013;39(4):782–95.
29. Yoshihara K, Shahmoradgoli M, Martínez E, Vegesna R, Kim H, Torres-Garcia W, Treviño V, Shen H, Laird PW, Levine DA, et al. Inferring tumour purity and stromal and immune cell admixture from expression data. Nat Commun. 2013;4(1):2612.
30. Paraskevopoulou MD, Georgakilas G, Kostoulas N, Vlachos IS, Vergoulis T, Reczko M, Filippidis C, Dalamagas T, Hatzigeorgiou AG. DIANA-microT web server v5.0: service integration into MiRNA functional analysis workflows. Nucleic Acids Res 2013, 41(Web Server issue):W169–173.
31. Nakagawa T, Tanaka Y, Matsuoka E, Kondo S, Okada Y, Noda Y, Kanai Y, Hirokawa N. Identification and classification of 16 new Kinesin superfamily (KIF) proteins in mouse genome. Proc Natl Acad Sci U S A. 1997;94(18):9654–9.
32. Yang Z, Li C, Yan C, Li J, Yan M, Liu B, Zhu Z, Wu Y, Gu Q. KIF14 promotes tumor progression and metastasis and is an independent predictor of poor prognosis in human gastric cancer. Biochim Biophys Acta Mol Basis Dis. 2019;1865(1):181–92.
33. Cheng C, Wu X, Shen Y, Li Q. KIF14 and KIF23 promote cell proliferation and chemoresistance in HCC cells, and predict worse prognosis of patients with HCC. Cancer Manag Res. 2020;12:13241–57.
34. Yang Z, Peng B, Pan Y, Gu Y. Analysis and verification of N(6)-methyladenosine-modified genes as novel biomarkers for clear cell renal cell carcinoma. Bioengineered. 2021;12(2):9473–83.
35. Tong K, Hu Z. FOXI1 expression in chromophobe renal cell carcinoma and renal oncocytoma: a study of the Cancer genome atlas transcriptome-based outlier mining and immunohistochemistry. Virchows Arch. 2021;478(4):647–58.
36. Nassar AH, Abou Alaiwi S, Baca SC, Adib E, Corona RI, Seo JH, Fonseca MAS, Spisak S, El Zarif T, Tisza V, et al. Epigenomic charting and functional annotation of risk loci in renal cell carcinoma. Nat Commun. 2023;14(1):346.
37. Feng H, Lane KA, Roumeliotis TI, Jeggo PA, Somaiah N, Choudhary JS, Downs JA. PBAF loss leads to DNA damage-induced inflammatory signaling through defective G2/M checkpoint maintenance. Genes Dev. 2022;36(13–14):790–806.
38. Clark DJ, Dhanasekaran SM, Petralia F, Pan J, Song X, Hu Y, da Veiga Leprevost F, Reva B, Lih TM, Chang HY, et al. Integrated proteogenomic characterization of clear cell renal cell carcinoma. Cell. 2019;179(4):964–e983931.

39. Du W, Zhang L, Brett-Morris A, Aguila B, Kerner J, Hoppel CL, Puchowicz M, Serra D, Herrero L, Rini BI, et al. HIF drives lipid deposition and cancer in ccRCC via repression of fatty acid metabolism. Nat Commun. 2017;8(1):1769.
40. Li H, Mo Z. Prognostic value of Metabolism-Related genes and immune infiltration in clear cell renal cell carcinoma. Int J Gen Med. 2021;14:6885–98.
41. Iglesias-Escudero M, Arias-González N, Martínez-Cáceres E. Regulatory cells and the effect of cancer immunotherapy. Mol Cancer. 2023;22(1):26.
42. Chu X, Tian Y, Lv C. Decoding the Spatiotemporal heterogeneity of tumor-associated macrophages. Mol Cancer. 2024;23(1):150.
43. Chen J, Duan Y, Che J, Zhu J. Dysfunction of dendritic cells in tumor microenvironment and immunotherapy. Cancer Commun (Lond). 2024;44(9):1047–70.
44. Angelin A, Gil-de-Gómez L, Dahiya S, Jiao J, Guo L, Levine MH, Wang Z, Quinn WJ 3rd, Kopinski PK, Wang L, et al. Foxp3 reprograms T cell metabolism to function in Low-Glucose, High-Lactate environments. Cell Metab. 2017;25(6):1282–e12931287.
45. Watson MJ, Vignali PDA, Mullett SJ, Overacre-Delgoffe AE, Peralta RM, Grebinoski S, Menk AV, Rittenhouse NL, DePeaux K, Whetstone RD, et al. Metabolic support of tumour-infiltrating regulatory T cells by lactic acid. Nature. 2021;591(7851):645–51.
46. Gong Z, Zhang J, Guo W. Tumor purity as a prognosis and immunotherapy relevant feature in gastric cancer. Cancer Med. 2020;9(23):9052–63.
47. Hinshaw DC, Shevde LA. The tumor microenvironment innately modulates Cancer progression. Cancer Res. 2019;79(18):4557–66.
48. Xie F, Xu M, Lu J, Mao L, Wang S. The role of Exosomal PD-L1 in tumor progression and immunotherapy. Mol Cancer. 2019;18(1):146.

Publisher's note